

Effect of Rb and Ta Doping on the Ionic Conductivity and Stability of the Garnet $\text{Li}_{7+2x-y}(\text{La}_{3-x}\text{Rb}_x)(\text{Zr}_{2-y}\text{Ta}_y)\text{O}_{12}$ ($0 \leq x \leq 0.375$, $0 \leq y \leq 1$) Superionic Conductor: A First Principles Investigation

Lincoln J. Miara,^{*,†} Shyue Ping Ong,[‡] Yifei Mo,[‡] William Davidson Richards,[‡] Youngsin Park,[§] Jae-Myung Lee,[§] Hyo Sug Lee,^{†,§} and Gerbrand Ceder[‡]

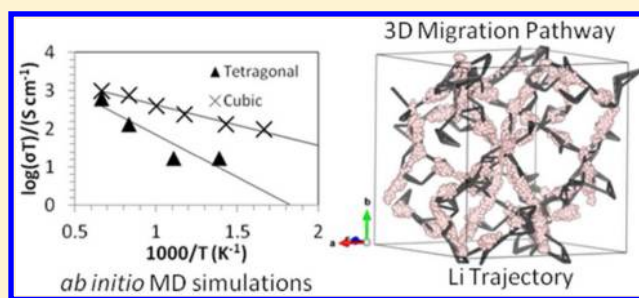
[†]Samsung Advanced Institute of Technology—USA, 1 Cambridge Center, Suite 702, Cambridge, Massachusetts 02142, United States

[‡]Department of Materials Science and Engineering, Massachusetts Institute of Technology, 77 Massachusetts Ave, Cambridge, Massachusetts 02139, United States

[§]Battery Group, Samsung Advanced Institute of Technology, Yongin 446-712, Republic of Korea

ABSTRACT: In this work, we investigated the effect of Rb and Ta doping on the ionic conductivity and stability of the garnet $\text{Li}_{7+2x-y}(\text{La}_{3-x}\text{Rb}_x)(\text{Zr}_{2-y}\text{Ta}_y)\text{O}_{12}$ ($0 \leq x \leq 0.375$, $0 \leq y \leq 1$) superionic conductor using first principles calculations. Our results indicate that doping does not greatly alter the topology of the migration pathway, but instead acts primarily to change the lithium concentration. The structure with the lowest activation energy and highest room temperature conductivity is $\text{Li}_{6.75}\text{La}_3\text{Zr}_{1.75}\text{Ta}_{0.25}\text{O}_{12}$ ($E_a = 19$ meV, $\sigma_{300\text{K}} = 1 \times 10^{-2}$ S cm^{-1}). All Ta-doped structures have significantly higher ionic conductivity than the undoped cubic $\text{Li}_7\text{La}_3\text{Zr}_2\text{O}_{12}$ (*c*-LLZO, $E_a = 24$ meV, $\sigma_{300\text{K}} = 2 \times 10^{-3}$ S cm^{-1}). The Rb-doped structure with composition $\text{Li}_{7.25}\text{La}_{2.875}\text{Rb}_{0.125}\text{Zr}_2\text{O}_{12}$ has a lower activation energy than *c*-LLZO, but further Rb doping leads to a dramatic decrease in performance. We also examined the effect of changing the lattice parameter at fixed lithium concentration and found that a decrease in the lattice parameter leads to a rapid decline in Li^+ conductivity, whereas an expanded lattice offers only marginal improvement. This result suggests that doping with larger cations will not provide a significant enhancement in performance. Our results find higher conductivity and lower activation energy than is typically reported in the experimental literature, which suggests that there is room for improving the total conductivity in these promising materials.

KEYWORDS: garnets, *ab initio* molecular dynamics, solid electrolyte, lithium ionic conductivity



INTRODUCTION

There is considerable interest in developing all solid-state Li-ion batteries (LIBs) as an alternative to traditional organic liquid electrolyte based LIBs. The primary difficulty has been to obtain an electrolyte that can simultaneously meet a strict set of demands: high ionic conductivity, low electronic conductivity, chemical compatibility with electrodes, a wide electrochemical operating voltage window, environmentally benign, and does not require a complex manufacturing process. A number of classes of materials have been identified that can partially satisfy this list of demands. For example, LiPON has a very wide stability window and is chemically compatible with elemental Li anodes.^{1,2} However, the conductivity is rather low ($\sim 10^{-6}$ S cm^{-1} at room temperature) requiring expensive thin film vapor deposition techniques.³ On the other hand, $\text{Li}_{10}\text{GeP}_2\text{S}_{12}$ (LGPS), a recently identified superionic conductor, has a conductivity of 12 mS cm^{-1} at room temperature that rivals many liquid electrolytes, and appears to be stable over a relatively wide operating voltage range.^{4,5} Yet it is a sulfide and rapidly decomposes with exposure to water forming toxic H_2S gas. To date the most promising class of materials appear to be

those crystallizing with a garnet like structure.⁶ The material $\text{Li}_7\text{La}_3\text{Zr}_2\text{O}_{12}$ satisfies most of the criteria necessary for a good electrolyte except that the room temperature conductivity ($\sim 10^{-4}$ S cm^{-1}) is still far lower than that of LGPS. This value is appropriate for thin batteries, but it is likely that $>10^{-2}$ S cm^{-1} is required for larger format batteries. Thus, much research has been focused on this system trying to improve the conductivity, while maintaining the other useful properties.

The garnet has the general formula $\text{A}_3\text{B}_3\text{C}_2\text{O}_{12}$ where B and C are cations respectively coordinated by eight and six oxygen atoms as shown in ref 7. A rigid three-dimensional (3D) framework is created by the $\text{B}_3\text{C}_2\text{O}_{12}$ moiety, and the A cation is able to distribute across face sharing octahedral and tetrahedral sites. Because the A site has a total of 72 tetrahedral and octahedral sites in the conventional unit cell of 8 formula units, more lithium can be accommodated. The compounds first identified as lithium ion conductors, by Thangadurai and

Received: April 16, 2013

Revised: June 20, 2013

Published: June 20, 2013

Weppner,⁸ are $\text{Li}_5\text{La}_3\text{M}_2\text{O}_{12}$ ($\text{M} = \text{Nb}, \text{Ta}$), which crystallize with an aristotype garnet space group $Ia\bar{3}d$ (Int. No. 230). However, the conductivities of these compounds are fairly low at about $10^{-6} \text{ S cm}^{-1}$ at room temperature. More recently, the compound $\text{Li}_7\text{La}_3\text{Zr}_2\text{O}_{12}$ (LLZO) was discovered as a lithium ion conductor.⁹ At room temperature, it has a tetragonal structure with space group $I4_1/abc$ (Int. No. 142).^{10,11} This compound also has poor conductivity (around $10^{-6} \text{ S cm}^{-1}$) because the Li are stabilized in low energy sites. However, it was shown that the cubic structure could be stabilized with the addition of about 0.2 Al per formula unit of LLZO, usually from the alumina crucibles used to fire it.^{12,13} The stabilized cubic structure has a room temperature conductivity $>10^{-4} \text{ S cm}^{-1}$.^{14–16} Thus the hunt for the optimal Li concentration that maximizes conductivity ensued, with compositions in the range $\text{Li}_x\text{La}_3\text{Zr}_2\text{O}_{12}$ ($5 \leq x \leq 7$) having been synthesized by doping both the La and the Zr sites with various cations, or doping the Li sites with additional Al.^{15,17–20} The result of doping has shown a reduction in sintering temperature with La site doping (Sr, Ba, or Ca), and improved conductivity by doping the Zr site (Ta, or Nb). Yet the results vary widely depending on synthesis conditions, and no clear consensus has emerged as to how doping affects the structure. Very recent experimental evidence suggests that additional lithium beyond $\text{Li} = 7.0/\text{FU}$ can be achieved by doping with Rb^+ on the La^{3+} site. Further, improved conductivity was shown for $\text{Li} = 7.25/\text{FU}$ producing a room temperature conductivity $\sim 8 \times 10^{-4} \text{ S cm}^{-1}$ and a low activation energy of 0.29 eV with a cold pressed pellet.²¹ However, because of the complex structure, the relationship between topology (i.e., the migration pathway), lithium concentration, and conductivity has been difficult to separate.

In this work, we investigate the effect of doping $\text{Li}_7\text{La}_3\text{Zr}_2\text{O}_{12}$ (LLZO) using ab initio methods and topology analysis. Doping of the LLZO structure with Ta on the Zr site and Rb on the La site generates structures with a lithium concentration range of $\text{Li} = 6–7.75/\text{FU}$. We study the impact of these composition changes on the migration pathways and diffusivity, and suggest ways to improve conductivity.

METHODS

Initial Structure Optimization. The low temperature stable phase of LLZO is the tetragonal structure (*t*-LLZO) with space group $I4_1/abc$ (Int. No. 142). This is an ordered structure with lithium on the 8a and 16f tetragonal sites and on the 32g octahedral sites. We obtained this structure from the ICSD (CC: 246816)²² and relaxed it computationally to obtain initial positions and lattice parameters for further simulation. The metastable cubic structure (*c*-LLZO) has been shown to be stabilized with a small amount of Al addition from the crucible used to make the original powder. This compound crystallizes with space group $Ia\bar{3}d$ (No. 230), and is disordered on both the 24d Li(1) tetragonal site and the 96h Li(2) octahedral sites (see Figure 1). We obtained the initial disordered structure from the ICSD (CC: 422259), which has reported site occupancy factors (SOFs) that are unlikely to be correct. While the exact site occupancy factors (SOFs) are unknown, the problem was recently examined computationally,^{23,24} and we adopted SOF values consistent with that work. We used SOF = 0.417 for Li(1) and 0.479 for Li(2).

To obtain initial structures for the simulations, we ordered the lithium atoms based on the SOFs using an electrostatic energy criterion²⁵ implemented in the Python Materials Genomics (pymatgen) analysis code.²⁶ First, the ions were assigned idealized charges, that is, Li^{1+} , La^{3+} , Zr^{4+} , and O^{2-} . Given the large number of possible permutations of Li positions, the Li sites were assigned using a simple strategy of removing Li sites with the highest electrostatic

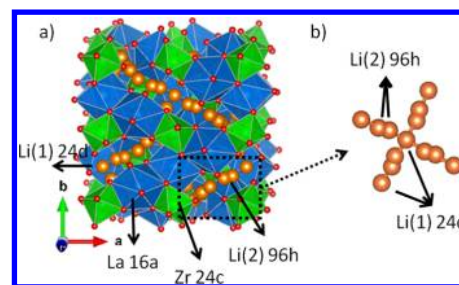


Figure 1. (a) Cubic garnet structure with space group $Ia\bar{3}d$ (Int. No. 142). The Li(1) are in tetrahedral 24d sites while Li(2) are in octahedral 96h sites. The La (blue) and Zr (red) are coordinated by 8- and 6- oxygen (red) respectively. (b) The 3D network of Li (brown) atoms is shown. The Li(1) site is surrounded by four Li(2) octahedral sites.

energy in sequence until the desired lithium concentrations were reached. We took this approach as opposed to finding the lowest electrostatic energy configuration since the number of possible combinations on the Li sites is tremendously high ($>10^{11}$). However, since we are mainly interested in the diffusion properties of these materials, in which case all of the Li ions are free to move within the Li network, finding the exact ground state Li arrangement was not a priority.

For doped compositions, a similar approach was adopted. In addition to ordering the lithium atoms, the dopants also had to be ordered. First the dopant was ordered to find the lowest electrostatic energy configurations, and then the lithium atoms were removed as described above to their respective concentrations. Thirty structures with the lowest electrostatic energy having different dopant arrangements, but a constant Li ordering were selected and relaxed with density functional theory (DFT). The structure with the lowest DFT energy was then chosen for the starting material for AIMD simulations.

All structures were relaxed using the Vienna Ab initio Simulation Package (VASP)²⁷ within the projector augmented-wave (PAW)²⁸ approach. The total energy calculations were performed using the Perdew–Burke–Ernzerhof (PBE) generalized-gradient approximation (GGA)²⁹ functional. A *k*-point density of at least 500/(number of atoms in the unit cell) was used for all computations.

Ab initio Molecular Dynamics Diffusivity Calculation. For the diffusivity and conductivity calculations, we used ab initio molecular dynamics (AIMD) simulations implemented in VASP. The PBE GGA functional was used. The computational cost was kept to a reasonable level by using a minimal Γ -centered $1 \times 1 \times 1$ *k*-point grid, a plane wave energy cutoff of 400 eV, and nonspin-polarized calculations. A $1 \times 1 \times 1$ unit cell was used, which corresponds to 8 formula units (i.e., 192 atoms for LLZO). The initial positions and unit cell volumes were obtained from the DFT calculations. The Verlet algorithm, as implemented in VASP, was used to solve Newton's equation of motion. The AIMD time step was 2 fs. The AIMD simulation procedure followed the same procedure as described in ref 5. Briefly, the structure was heated from 100 K to the desired temperature. It was then allowed to equilibrate for 10 ps in the NVT ensemble with a Nose–Hoover thermostat. MD simulations were performed to determine diffusion coefficients for 40 to 100 ps in the NVT ensemble until they were converged. We determined the self-diffusion coefficient, D , of Li^+ as the ensemble mean squared displacement over time t , as follows

$$D = \frac{1}{2dt} \langle [r(t)]^2 \rangle$$

Where d equals 3, the dimension in the lattice through which diffusion occurs, and $\langle [r(t)]^2 \rangle$ is the mean squared displacement (MSD) of the Li atoms. The value of D was obtained by performing a linear fitting of the MSD vs $2dt$. Activation energies were determined from Arrhenius plots of the diffusivity. To estimate room temperature conductivity,

which allows us to compare data with experimental results, we assumed uncorrelated motion and used the Nernst–Einstein equation. There is evidence of short-range Li–Li correlated motion;^{24,30} however, classical MD results suggest that the longer range 3D transport is relatively uncorrelated with a Haven Ratio in the range 0.5–1 in *c*-LLZO.²⁴

Topology Analysis. Topological analysis was performed using the Zeo++ software,³¹ which constructs the Voronoi tessellation of a periodic crystal system and returns key system parameters. We determined the migration channel of the DFT relaxed structures by removing all the lithium in the system and then analyzing the remaining void space. The migration channel was constructed by finding connected nodes and edges that are large enough to accommodate a lithium atom. If the connected nodes pass through the entire unit cell in at least one direction, then a migration channel is said to exist. One way to characterize the migration pathway is to examine the radius of the narrowest channel in the pathway. We designate this as the bottleneck size, R_B , and it was determined as the largest free sphere which could pass through the 3-dimensional migration channel. The void space was divided into migration channels, which are connected throughout the cell, and inaccessible regions, which are large enough to accommodate lithium, but are not connected to the main pathway.

RESULTS

Structural Stability. It is critical for any new or hypothetical compound that one evaluates the thermodynamic stability. Stability of a compound needs to be performed against all possible linear combinations of compounds in this compositional space, and can be evaluated by the convex hull construction.³² In this case this analysis requires the energy of all known compounds in the quaternary Li–La–Zr–O–M ($M = \text{Ta or Rb}$) phase diagram. Table 1 shows the thermodynamic

Table 1. Equilibrium Decomposition Products and Decomposition Energies for

$\text{Li}_{56+2x-y}(\text{La}_{24-x}\text{Rb}_x)(\text{Zr}_{16-y}\text{Ta}_y)\text{O}_{96}$ ($0 \leq x \leq 3$, $0 \leq y \leq 8$)

[dopant]	equilibrium decomposition products ^a	E_{decomp} (meV per atom)
$\text{Ta}_y = 8.0$	$1.33\text{La}_2\text{Zr}_2\text{O}_7 + 9\text{La}_2\text{O}_3 + 8\text{Li}_5\text{TaO}_5 + 2.67\text{Li}_6\text{Zr}_2\text{O}_7$	4
6.0	$1.67\text{La}_2\text{Zr}_2\text{O}_7 + 10\text{La}_2\text{O}_3 + 6\text{Li}_5\text{TaO}_5 + 3.33\text{Li}_6\text{Zr}_2\text{O}_7$	11
4.0	$0.67\text{La}_2\text{Zr}_2\text{O}_7 + 11\text{La}_2\text{O}_3 + 4\text{Li}_5\text{TaO}_5 + 5.33\text{Li}_6\text{Zr}_2\text{O}_7$	15
2.0	$0.4\text{Li}_8\text{ZrO}_6 + 12\text{La}_2\text{O}_3 + 2\text{Li}_5\text{TaO}_5 + 6.8\text{Li}_6\text{Zr}_2\text{O}_7$	18
<i>c</i> -LLZO	$1.6\text{Li}_8\text{ZrO}_6 + 7.2\text{Li}_6\text{Zr}_2\text{O}_7 + 12\text{La}_2\text{O}_3$	18
<i>t</i> -LLZO	$1.6\text{Li}_8\text{ZrO}_6 + 7.2\text{Li}_6\text{Zr}_2\text{O}_7 + 12\text{La}_2\text{O}_3$	3
$\text{Rb}_x = 1.0$	$\text{RbLaO}_2 + 11\text{La}_2\text{O}_3 + 2\text{Li}_8\text{ZrO}_6 + 7\text{Li}_6\text{Zr}_2\text{O}_7$	3
2.0	$2\text{RbLaO}_2 + 10\text{La}_2\text{O}_3 + 2.4\text{Li}_8\text{ZrO}_6 + 6.8\text{Li}_6\text{Zr}_2\text{O}_7$	6
3.0	$3\text{RbLaO}_2 + 9\text{La}_2\text{O}_3 + 2.8\text{Li}_8\text{ZrO}_6 + 6.6\text{Li}_6\text{Zr}_2\text{O}_7$	20

^aFor Unit Cell with $\text{Li}_{56+2x-y}(\text{La}_{24-x}\text{Rb}_x)(\text{Zr}_{16-y}\text{Ta}_y)\text{O}_{96}$ ($0 \leq x \leq 3$, $0 \leq y \leq 8$).

phase equilibria determined for $\text{Li}_{7+2x-y}(\text{La}_{3-x}\text{Rb}_x)(\text{Zr}_{2-y}\text{Ta}_y)\text{O}_{12}$ ($0 \leq x \leq 0.375$, $0 \leq y \leq 1$) in the appropriate phase diagram. The stability is given as the calculated driving force for decomposition into the ground state products. As described in more detail elsewhere,⁵ the decomposition energy is the negative of the reaction energy per atom to decompose into the equilibrium products. Thus, stable compounds have $E_{\text{decomp}} = 0$,

and the higher the E_{decomp} the less likely a structure is to be stable; all decomposition energies are given per atom.

All of the compounds in the $\text{Li}_{7+2x-y}(\text{La}_{3-x}\text{Rb}_x)(\text{Zr}_{2-y}\text{Ta}_y)\text{O}_{12}$ ($0 \leq x \leq 0.375$, $0 \leq y \leq 1$) series are predicted to be metastable. It is generally considered that entropic effects can stabilize compounds with decomposition energies below about 25 meV, and it is likely that all structures here can be synthesized. Several interesting trends are apparent from the data. First, *c*-LLZO is 18 meV above the ground state products whereas *t*-LLZO is only 3 meV above this hull. This is in good agreement with the experimental findings that the tetragonal form is the stable ground state of LLZO. The addition of Ta works to increasingly stabilize the cubic structure, such that at $\text{Ta}_y = 1.0$, E_{decomp} is only 4 meV. This result is in agreement with X-ray diffraction (XRD) results which show that the pure Ta compound, $\text{Li}_5\text{La}_3\text{Ta}_2\text{O}_{12}$, is cubic.³³ Interestingly, for Rb doping, the least doped structure is the most stable. Adding more Rb causes the structure to become increasingly metastable. This is a possible indication that the solubility of Rb may be limited.

The decomposition products of LLZO are Li_8ZrO_6 , $\text{Li}_6\text{Zr}_2\text{O}_7$, and La_2O_3 . The first two are known lithium ionic conductors³⁴ while La_2O_3 would be expected to act as an insulating phase. At $\text{Ta}_y = 0.25$ the decomposition product Li_5TaO_5 appears which is also expected to be an ion conductor.³⁵ However, further addition of Ta stabilizes the formation of $\text{La}_2\text{Zr}_2\text{O}_7$ which would act as an insulating phase. Rb addition creates RbLaO_2 as a decomposition product which would act as an insulator.

Lithium Diffusivity and Conductivity. Figure 2a shows Arrhenius plots for the conductivity for both tetragonal (*t*-LLZO) and cubic (*c*-LLZO) $\text{Li}_7\text{La}_3\text{Zr}_2\text{O}_{12}$. The tetragonal phase has a calculated activation energy of 0.43 eV and $\sigma_{300\text{K}}$ of 1×10^{-6} S/cm. This result is in excellent agreement with values from classical MD simulations³⁶ and with recent experimental results.¹⁸ The cubic phase has a significantly lower calculated activation energy of 0.24 eV, and higher conductivity of $\sigma_{300\text{K}} = 2 \times 10^{-3}$ S/cm. The calculated activation energy for the cubic phase is lower, and the calculated conductivity value is higher than the typical experimental values of $E_a = 0.29\text{--}0.4$ eV and $\sigma_{298} = (1\text{--}4) \times 10^{-4}$ S cm^{-1} , but is in close agreement with the calculated activation energy from NEB calculations of 0.26 eV.³⁷ This difference between calculations and experiment is explained in the Discussion section. However, the relative differences between *c*- and *t*-LLZO correspond well with the experimental evidence that the cubic phase is a significantly better conductor than the tetragonal phase, and thus AIMD with an NVT ensemble appears to adequately simulate the system.

The effect of Rb^+ doping on conductivity is shown as an Arrhenius plot in Figure 2b. The calculated activation energy, $\sigma_{300\text{K}}$, bottleneck size, and lattice parameters from DFT are summarized in Table 2. At $[\text{Li}] = 7.5/\text{FU}$, the activation energy is very high, and no diffusion was seen below 1000 K during our simulation time. At this concentration, lithium fully occupies the low energy sites, and so they are stabilized and unable to move except at extremely high temperatures. As more lithium is accommodated, at $[\text{Li}] = 7.75/\text{FU}$, the conductivity increases. From an analysis of the trajectory and topology, there is no evidence of a change in the migration pathway, so it is the increased concentration that appears to destabilize the lithium and push them into higher energy sites allowing for some lithium diffusion to occur. The activation energy at $[\text{Li}] = 7.25/$

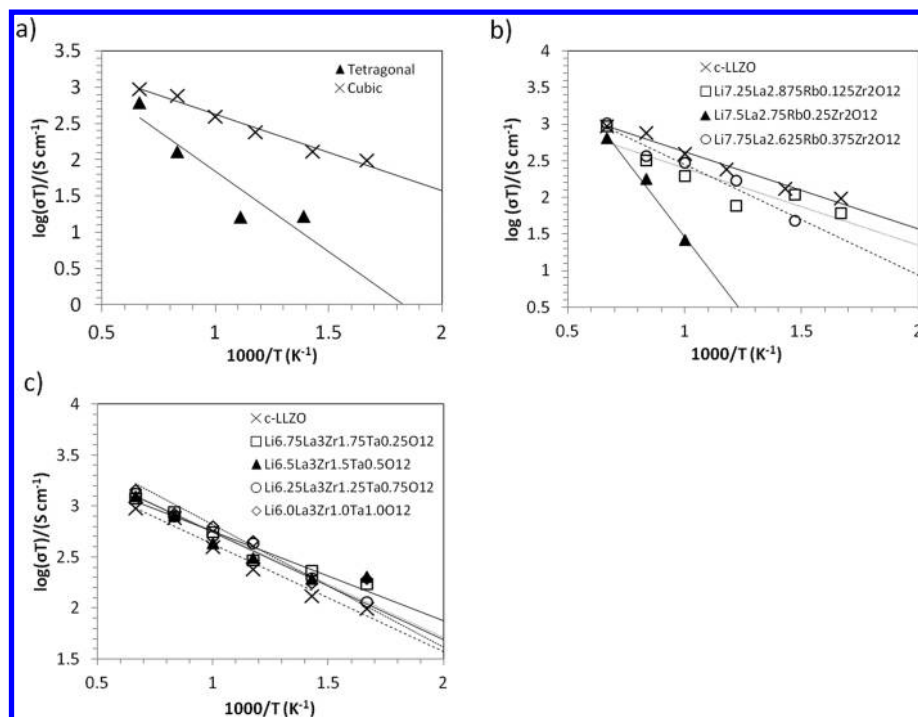


Figure 2. Arrhenius plots for σT obtained with AIMD simulation and showing (a) the tetragonal phase has an activation energy of 0.43 eV and $\sigma_{300\text{K}} = 1 \times 10^{-6}$ S/cm. The cubic phase has an activation energy of 0.24 and $\sigma_{300\text{K}} = 1 \times 10^{-3}$ S/cm. (b) The Rb doped structures, and (c) the Ta doped structures.

Table 2. Conductivity and Relaxed Parameters for the Doped Structures in the Series $\text{Li}_{56+2x-y}(\text{La}_{24-x}\text{Rb}_x)(\text{Zr}_{16-y}\text{Ta}_y)\text{O}_{96}$ ($0 \leq x \leq 3, 0 \leq y \leq 8$)

[dopant]	E_a (eV)	$\sigma_{300\text{K}}$ (S cm $^{-1}$)	R_B (Å)	Vol. (Å 3)	a (Å)	b (Å)	c (Å)	
Tay =	8.0	0.20 ± 0.015	1.05×10^{-02}	1.327	2170.89	12.941	12.932	12.956
	6.0	0.19 ± 0.009	1.14×10^{-02}	1.314	2183.17	13.023	12.936	12.959
	4.0	0.20 ± 0.039	9.71×10^{-03}	1.316	2200.54	13.137	12.913	12.972
	2.0	0.19 ± 0.020	1.17×10^{-02}	1.317	2212.86	13.145	12.961	12.988
c-LLZO		0.24 ± 0.022	2.40×10^{-03}	1.314	2223.45	13.116	13.070	12.971
Rbx =	1.0	0.21 ± 0.026	2.74×10^{-03}	1.317	2247.73	13.013	13.161	13.015
	2.0	0.48 ± 0.114	3.35×10^{-07}	1.321	2266.65	13.121	13.073	13.086
	3.0	0.30 ± 0.023	2.81×10^{-04}	1.326	2297.72	13.126	13.233	13.112

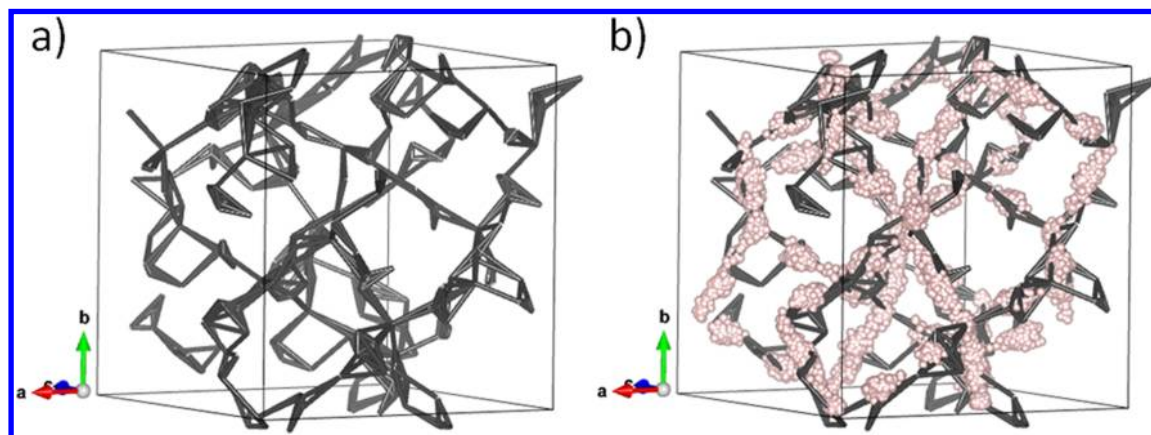


Figure 3. Results from (a) the migration pathway identified from topology analysis, and (b) the AIMD trace at 600 K for *c*-LLZO showing that the predicted pathway from topology closely agrees with the AIMD trace, all hops follow the Li(2)–Li(1)–Li(2) trajectory, no Li(2)–Li(2) hops are observed.

FU is 0.21 eV, which is lower than *c*-LLZO. The calculated Arrhenius plot for the Ta-doped structures is shown in Figure 2c. All doped structures show enhanced conductivity compared

to *c*-LLZO. The maximum occurs at [Li] = 6.75/FU, in good agreement with previous experimental results.¹⁸ At this concentration, the activation energy is 0.19 eV and $\sigma_{300\text{K}} =$

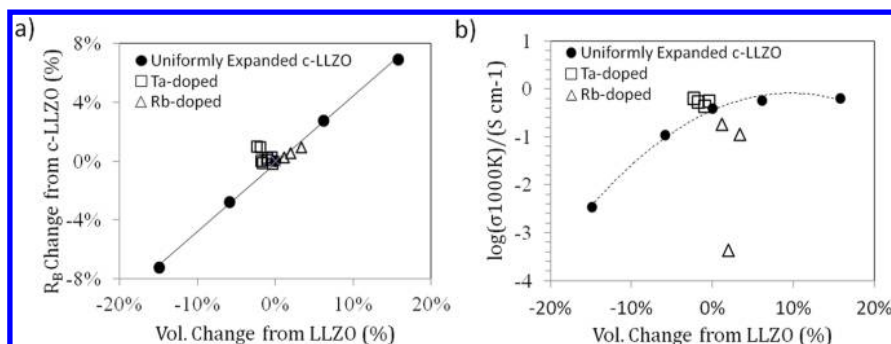


Figure 4. Effect of topology is isolated from concentration effects. Panel a shows the change in bottleneck size when the LLZO structure is uniformly expanded or contracted. For comparison, the volume and bottleneck size for the Ta and Rb-doped structures are plotted as squares (\square) and triangles (\triangle), respectively. Panel b shows the conductivity at 1000 K for the uniformly expanded LLZO and the doped structures. A rapid decline with constriction is evident, while only moderate improvement with lattice parameter expansion is seen. The dashed line is only shown for clarity.

$12 \times 10^{-3} \text{ S cm}^{-1}$. This is in excellent agreement with the reported values of $E_a = 0.22 \text{ eV}$ and $\sigma_{298} = 0.9 \times 10^{-3} \text{ S cm}^{-1}$ on a hot pressed $\text{Li}_{6.75}\text{La}_3(\text{Zr}_{1.75}\text{Ta}_{0.25})\text{O}_{12}$ sample.¹⁸ The other concentrations in this series also have high conductivity and low activation energy.

Topology Analysis. The migration pathway identified through topology analysis predicts a 3D migration pathway in which the lithium moves along a pathway from $-\text{Li}(2)-\text{Li}(2)-\text{Li}(1)-\text{Li}(2)-$ as shown with an AIMD trace in Figure 3a, the fixed atoms indicate the location of the Wyckoff sites. However, it is not necessary to pass through the center of the tetrahedrons as there is space large enough for the lithium to pass through the corner without reaching the actual 24d site. This agrees with previous NEB and AIMD results.^{37,23} The ionic radius of $\text{Ta}^{5+} = 0.78 \text{ \AA}$ is 9% smaller than $\text{Zr}^{4+} = 0.86 \text{ \AA}$, and that of $\text{Rb}^{1+} = 1.66 \text{ \AA}$ is 42% larger than $\text{La}^{3+} = 1.17 \text{ \AA}$. Thus, doping with Ta^{5+} causes up to a 2% reduction ($[\text{Li}] = 6-6.25/\text{FU}$) in the relaxed unit cell volume, while Rb^{1+} doping increases the unit cell volume up to 3% at $[\text{Li}] = 7.75/\text{FU}$. The effect on the bottleneck size with Rb^{1+} doping is more modest, with only a 1% expansion seen at $[\text{Li}] = 7.75/\text{FU}$, whereas very little change is observed below $[\text{Li}] = 7.5/\text{FU}$ compared to the c-LLZO structure. Interestingly, at the lowest lithium concentration ($[\text{Li}] = 6.0/\text{FU}$), there is a 1% expansion in the bottleneck size compared to c-LLZO despite an overall volume reduction. This is the result of a shift in the oxygen positions associated with the Ta octahedron, creating a slight enlargement of the bottleneck. The nature of the void space is characterized by accessible and inaccessible regions. In the lithium concentration range from $[\text{Li}] = 6-7.25$, we see a fully connected accessible migration pathway. However, at $[\text{Li}] = 7.5/\text{FU}$ and beyond, we see regions becoming inaccessible to lithium migration because of the relaxation of the cation polyhedra that shift into the migration pathway. Nonetheless, the overall pathway remains largely the same. This suggests that the primary effect of doping, in the investigated region, is to change the lithium concentration while the bottleneck size and migration pathway are relatively unaffected.

From Figure 3(a,b), we may observe that the migration pathway identified from a topological analysis closely agrees with the lithium trajectories along the pathway: $\text{Li}(2)-\text{Li}(1)-\text{Li}(2)$, with no direct hops from one octahedron to the next through the shared edge. This agrees with ref 37 and neutron diffraction studies,³⁸ and validates topology analysis as a useful method to identify migration pathways.

Effect of Topology on Diffusivity. To check if an enlarged migration pathway would enhance diffusivity, we uniformly expanded the c-LLZO lattice parameter by $\pm 5\%$. The effect on volume change and bottleneck size compared to the doped structures is shown in Figure 4a. The conductivity at 1000 K was then calculated and is plotted in Figure 4b. A significant drop-off in conductivity is seen when the lattice is constricted, and at a 5% reduction in lattice parameter, there is very little observed diffusion as the small bottleneck greatly increases the barrier for diffusion. With expansion, on the other hand, we only see a modest increase in conductivity. While some improvement is seen with expansion, the improvement is not large.

Lithium Distribution. When substituting Rb^{1+} on a La^{3+} site, it is necessary to add lithium to maintain charge neutrality. In the $Ia\bar{3}d$ crystal structure, the Li are located on a 96h octahedral site furthest from a neighboring occupied 24d tetrahedral site, and close to an empty neighboring 24d site.¹⁷ In this configuration, a total of $[\text{Li}] = 7.5/\text{FU}$ can be accommodated. However, for a structure with $[\text{Li}] = 7.75/\text{FU}$, to minimize the close Li-Li distances, a structure with bifurcated sites is observed. The lithium ions are arranged in a zigzag pattern with the Li atoms pushed from their ground state sites such that the neighboring lithium are as far apart as possible (Figure 5). In this manner, it is possible to have an occupied $\text{Li}(1)-\text{Li}(2)-\text{Li}(1)$ arrangement that does not exist for compositions below $\text{Li} = 7.75/\text{FU}$. From a radial distribution function analysis of the AIMD results, we find that the minimum Li-Li distance is 2.3 \AA , which is only slightly shorter than 2.6 \AA for the LLZO material. The minimum Li-O

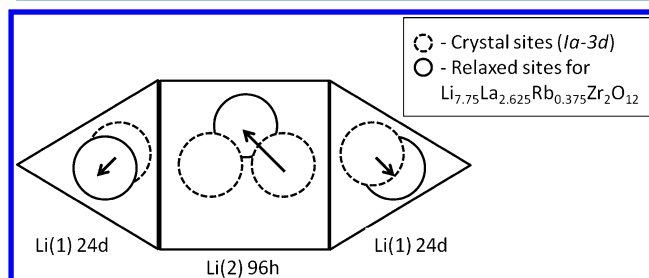


Figure 5. Figure showing Li shifting from low energy sites in the $Ia\bar{3}d$ crystal (dashed circle) to high energy sites (shaded circle) in $\text{Li}_{7.75}\text{La}_{2.625}\text{Rb}_{0.375}\text{Zr}_2\text{O}_{12}$ allowing occupation of neighboring $\text{Li}(1)-\text{Li}(2)-\text{Li}(1)$ sites while maintaining minimum Li-Li distances greater than 2.3 \AA .

distance for each of the three adjacent occupied sites ($-\text{Li}(1)-\text{Li}(2)-\text{Li}(1)-$) decreases slightly from the average in *c*-LLZO of 1.9 Å to $\text{Li}(1)-\text{O} = (1.848 \text{ \AA})$, $\text{Li}(2)-\text{O} = (1.852 \text{ \AA})$, $\text{Li}(1)-\text{O} = (1.872 \text{ \AA})$.

The distribution of lithium between the octahedral and the tetrahedral sites has been explored in the lithium concentration range: 5–7/FU by neutron diffraction^{30,39} as well as computationally for LLZO and $[\text{Li}] = 6.75/\text{FU}$.^{23,36} We looked at site occupancy in our MD simulations at different Li concentration as well as different temperatures. We determine the character of a Li site by determining the coordination of oxygen for a 3 Å radius around a given Li. High temperature SOFs were obtained as the average coordination during the course of the simulation. The results of the average occupation at 600 K during the simulation is shown in Figure 6a. There are two 96h

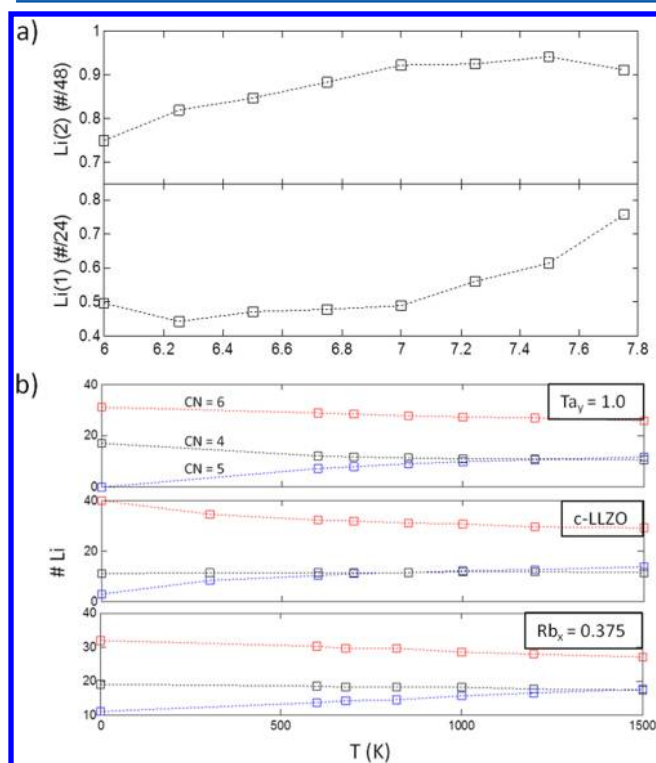


Figure 6. In (a) the average SOF is determined at 600 K for the different lithium concentrations at both the Li(1) and Li(2) sites. In (b) the average SOF is shown at different temperatures for $\text{Ta}_y = 1/0$ (top), *c*-LLZO (middle) and $\text{Rb}_x = 0.375$ (bottom).

sites per octahedron, but since they cannot be simultaneously occupied, we use the convention adopted in ref 37 and define the Li(2) SOF per octahedron, and thus 48 lithium in octahedral sites correspond to Li(2) SOF = 1. At 600 K, it is seen that the tetrahedral SOF is roughly constant at 0.5 between Li = 6.0 and 7.0/FU in agreement with previous work, and the lithium atoms are added to the octahedral site, suggesting vacancy ordering on the tetrahedral site. However, after Li = 7.0/FU, the zigzag structure (Figure 5) arises as the tetrahedral site is again disordered. These results differ from those predicted by Xie et al. who suggest that the maximal lithium concentration is Li = 7.5 at which point the vacancies are fully ordered on half of the Li(1) sites, and the octahedral sites are fully occupied.

As has been previously observed, there is a 5-fold coordinated site (CN = 5), which is a high energy site located

at the boundary between the tetragonal and octahedral site.³⁷ It results from a lithium pushed to the boundary between the Li(1) and Li(2) sites (see Figure 2 in ref 37). The occupation of this site is increasingly favored at elevated temperatures (see Figure 6b), whereas the CN = 6, within the octahedron, SOF declines. This suggests that the CN = 5 site is a high energy site, where a lithium atom rests before passing through a tetragonal site when a neighboring octahedral becomes available.

DISCUSSION

$\text{Li}_7\text{La}_3\text{Zr}_2\text{O}_{12}$ shows great promise as a solid state electrolyte for all solid state lithium ion batteries because of its stability against lithium metal anodes and wide electrochemical operating window. However, the room temperature conductivity typically observed in experiments is about $10^{-4} \text{ S cm}^{-1}$, which is too low for large format batteries. In an attempt to increase conductivity, researchers have reported success with aliovalent substitutions on both the La site and the Zr site. The reasons for performance improvement, however, have not been fully elucidated. We investigated the effect of changing the lithium concentration of $\text{Li}_{7+2x-y}(\text{La}_{3-x}\text{Rb}_x)(\text{Zr}_{2-y}\text{Ta}_y)\text{O}_{12}$ ($0 \leq x \leq 0.375$, $0 \leq y \leq 1$) on conductivity and the topology of the migration pathway. In general, we find that the topology, that is the bottleneck size and migration pathways, remains largely unchanged with doping whereas the conductivity varies significantly depending on concentration.

We first compared the conductivity of *t*-LLZO vs *c*-LLZO and saw a significant enhancement in conductivity for the cubic system. This is in good agreement with experimental evidence. However, the calculated values from DFT simulations show a better performing system than is typically observed experimentally. This improvement is likely a combination of two factors. First, most experiments underestimate the bulk conductivity because of inseparable contributions from the grain boundary resistance in impedance spectroscopy results. Allen et al. have demonstrated significantly enhanced performance using hot pressing to achieve dense pellets of roughly 98% of theoretical density, as opposed to results on pellets from conventional cold pressing, which are generally closer to 80% of theoretical density.¹⁸ The second reason is that our simulations are carried out at high temperatures ($>300 \text{ }^\circ\text{C}$), and it is possible that the activation energy changes closer to room temperature. This is supported by classical MD results.³⁶

All Ta-doped compounds have a higher conductivity than the undoped *c*-LLZO, and the maximum is seen at Li = 6.75/FU which agrees well with experimental evidence. The Ta doping also stabilizes the cubic structure as is shown by the decomposition energy calculations. For all Ta-doped structures, the activation energy is about 0.20 eV whereas the conductivity increases with doping concentration. This suggests that mechanism of conduction is the same, but the increased lithium concentration is largely responsible for the increased conductivity.

We make the novel finding that at $\text{Rb}_x = 0.125$, Rb doping slightly increases conductivity and slightly decreases the activation energy compared to the undoped *c*-LLZO. Further, adding this small amount of Rb acts to stabilize the cubic lattice, as seen by the very small decomposition energy. Because the octahedral sites are almost fully occupied in this structure, the extra lithium is accommodated in tetrahedral sites. It appears that this configuration forces the lithium to be in a higher energy arrangement, and thus improves performance, since it

cannot be explained by an expanded bottleneck or changes in the migration pathway, and the high site occupancy would be expected to increase the activation energy. When $x = 0.25$, all of the low energy sites become filled with Li and there is no diffusion except at the highest temperatures, with a very high activation energy. Interestingly, further doping to $x = 0.375$ appears to be a stable composition as there are no unphysical Li–Li bond distances from a radial pair distribution analysis. The extra lithium creates a bifurcated structure pushing the lithium out of their crystallographic sites making a zigzag pattern. This in turn leads to an increase in conductivity compared to the $x = 0.25$ structure. The differences we see in conductivity are shown to be related to differences in lithium concentration and are not likely related to the minor topological differences.

Finally, we isolated the effect of topology on conductivity by artificially changing the lattice parameter of *c*-LLZO by $\pm 5\%$. Contraction of the cell caused a rapid decline in conductivity, which can be related to a high energy barrier of passing through the constricted bottleneck. However, expanding the lattice parameter has little effect on conductivity. This suggests that the garnet framework is already nearly optimized to support rapid lithium diffusion.

CONCLUSIONS

In conclusion, we used AIMD and topology analysis to explore the effect of changing the lithium concentration and bottleneck size in LLZO. LLZO is a highly promising material for use as solid electrolyte; however, because of its complexity, understanding the effect of doping on conductivity has proven difficult experimentally.

Our results show that the primary effect of doping with either Ta or Rb, within the concentration range $\text{Li} = 6\text{--}7.75/\text{FU}$, is to change the lithium concentration rather than the size or nature of the migration pathway. This results in a conductivity vs concentration profile which increases slightly with higher lithium concentration; the conductivity maximum and activation energy minimum is seen at $\text{Li} = 6.75/\text{FU}$ where $\sigma_{300\text{K}} = 12 \text{ mS cm}^{-1}$ and $E_a = 0.19 \text{ eV}$. Further, we demonstrate that a small amount of Rb stabilizes the cubic crystal structure and improves performance. At $\text{Li} = 7.25/\text{FU}$ the performance is better than the undoped structure with an activation energy of 0.21 eV , and $\sigma_{300\text{K}} = 2.7 \text{ mS cm}^{-1}$. However, beyond this concentration, the conductivity rapidly declines because of a lack of vacancies. The topology of the *c*-LLZO migration pathway appears to be optimized since uniformly changing the lattice parameter causes a rapid decrease in conductivity when the bottleneck is constricted, but relatively little improvement is seen with increased lattice parameter.

Our simulations suggest that the doped *c*-LLZO is an excellent lithium ion conductor, with low activation energy. It appears that conductivity improvements can be expected by reducing the grain boundary resistance further improving this already promising material.

AUTHOR INFORMATION

Corresponding Author

*E-mail: lincoln.m@samsung.com.

Notes

The authors declare no competing financial interest.

ACKNOWLEDGMENTS

The authors would like to thank Samsung Advanced Institute of Technology for funding support on this research.

REFERENCES

- (1) Bates, J.; Dudney, N.; Gruzalski, G.; Zuhr, R. *Solid State Ionics*. **1992**, *56*, 647–654.
- (2) Yu, X. *J. Electrochem. Soc.* **1997**, *144*, 524.
- (3) Knauth, P. *Solid State Ionics*. **2009**, *180*, 911–916.
- (4) Kamaya, N.; Homma, K.; Yamakawa, Y.; Hirayama, M.; Kanno, R.; Yonemura, M.; et al. *Nat. Mater.* **2011**, *10*, 682–686.
- (5) Ong, S. P.; Mo, Y.; Richards, W. D.; Miara, L.; Lee, H. S.; Ceder, G. *Energy Environ. Sci.* **2013**, *6* (1), 148–156.
- (6) Thangadurai, V.; Weppner, W. *Ionics* **2006**, *12*, 81–92.
- (7) Li, Y.; Wang, C.-A.; Xie, H.; Cheng, J.; Goodenough, J. B. *Electrochem. Commun.* **2011**, *13*, 1289–1292.
- (8) Thangadurai, V.; Kaack, H.; Weppner, W. *J. F. ChemInform* **2003**, *34*, 437–440.
- (9) Murugan, R.; Thangadurai, V.; Weppner, W. *Angew. Chem., Int. Ed.* **2007**, *46*, 7778–81.
- (10) Awaka, J.; Kijima, N.; Hayakawa, H.; Akimoto, J. *J. Solid State Chem.* **2009**, *182*, 2046–2052.
- (11) Percival, J.; Kendrick, E.; Smith, R. I.; Slater, P. R. *Dalton Trans.* **2009**, 5177–5181.
- (12) Geiger, C. A.; Alekseev, E.; Lazic, B.; Fisch, M.; Armbruster, T.; Langner, R.; et al. *Inorg. Chem.* **2011**, *50*, 1089–1097.
- (13) Buschmann, H.; Dolle, J.; Berendts, S.; Kuhn, A.; Bottke, P.; Wilkening, M.; et al. *Phys. Chem. Chem. Phys.* **2011**, *13* (43), 19378–19392.
- (14) Murugan, R.; Ramakumar, S.; Janani, N. *Electrochem. Commun.* **2011**, 12–14.
- (15) Wang, Y.; Lai, W. *Electrochem. Solid-State Lett.* **2012**, *15*, A68.
- (16) Awaka, J.; Takashima, A.; Kataoka, K.; Kijima, N.; Idemoto, Y.; Akimoto, J. *Chem. Lett.* **2011**, *40*, 60–62.
- (17) Li, Y.; Wang, C.-A.; Xie, H.; Cheng, J.; Goodenough, J. B. *Electrochem. Commun.* **2011**, *13*, 1289–1292.
- (18) Allen, J. L.; Wolfenstine, J.; Rangasamy, E.; Sakamoto, J. *J. Power Sources* **2012**, *206*, 315–319.
- (19) Thangadurai, V.; Weppner, W. *J. Power Sources* **2005**, *142*, 339–344.
- (20) Narayanan, S.; Epp, V.; Wilkening, M.; Thangadurai, V. *RSC Adv.* **2012**, *2*, 2553.
- (21) Lee, J.-M.; Kim, T. Y.; Baek, S.-W. Fast Lithium Ion Conductor of $\text{Li}_{7+x}\text{M}_x\text{La}_{3-x}\text{Zr}_2\text{O}_{12}$ Compositions Having Garnet-type Structure. *MRS Meeting Abstract*; **2012**, J13.02.
- (22) *Inorganic Crystal Structure Database (ICSD) v. 2012*; The National Institutes of Science and Technology (NIST), Fachinformationszentrum: Karlsruhe (FIZ), Germany, 2012; http://www.fiz-karlsruhe.com/icsd_home.html.
- (23) Jalem, R.; Yamamoto, Y.; Shiiba, H.; Nakayama, M.; Munakata, H.; Kasuga, T.; Kanamura, K. *Chem. Mater.* **2013**, *25* (3), 425–430.
- (24) Adams, S.; Rao, R. P. *J. Mater. Chem.* **2012**, 1426–1434.
- (25) Ewald, P. P. *Ann. Phys.* **1921**, *64*, 253–287.
- (26) Ong, S. P.; Richards, W. D.; Jain, A.; Hautier, G.; Kocher, M.; Cholia, S.; et al. *Comput. Mater. Sci.* **2013**, *68*, 314–319.
- (27) Kresse, G.; Furthmüller, J. *Phys. Rev. B: Condens. Matter* **1996**, *54*, 11169–11186.
- (28) Blöchl, P. E. *Phys. Rev. B* **1994**, *50*, 17953.
- (29) Perdew, J.; Emzerhof, M.; Burke, K. *J. Chem. Phys.* **1996**, *105*, 9982–9985.
- (30) O’Callaghan, M. P.; Cussen, E. J. *Chem. Commun.* **2007**, 0, 2048–2050.
- (31) Willems, T. F.; Rycroft, C. H.; Kazi, M.; Meza, J. C.; Haranczyk, M. *Microporous Mesoporous Mater.* **2011**, *149*, 134–141.
- (32) Marrone, T. J.; Briggs, J. M.; McCammon, J. A. *Annu. Rev. Pharmacol. Toxicol.* **1997**, *37*, 71–90.
- (33) Thangadurai, V.; Kaack, H.; Weppner, W. *J. F. ChemInform* **2003**, *34*, 437–440.

- (34) Pantyukhina, M. I.; Shchelkanova, M. S.; Stepanov, a. P.; Buzlukov, a. L. *Bull. Russ. Acad. Sci.: Phys.* **2010**, *74*, 653–655.
- (35) Greaves, C.; Katib, S. *J. Chem. Soc., Chem. Commun.* **1987**, 5–6.
- (36) Adams, S.; Rao, R. P. *J. Mater. Chem.* **2012**, 1426–1434.
- (37) Xu, M.; Park, M. S.; Lee, J. M.; Kim, T. Y.; Park, Y. S.; Ma, E. *Phys. Rev. B* **2012**, *85*, 052301.
- (38) Han, J.; Zhu, J.; Li, Y.; Yu, X.; Wang, S.; Wu, G. *Chem. Commun. (Cambridge, U. K.)* **2012**, *48*, 9840–2.
- (39) Xie, H.; Alonso, J. A.; Li, Y.; Fernandez-Díaz, M. T.; Goodenough, J. B. *Chem. Mater.* **2011**, *23*, 3587–3589.